almost no effect on the value of η: the difference between the η-values for a patch (broken curve) and a dipole (dotted curve) is less than 0·02 for $\varepsilon_r = 2.55$, and nearly zero for $\varepsilon_r = 12.8$. As we are only interested in resonant antennas, the length L of the patch is not of importance: it is determined by W, h, ε_r and the resonant frequency. Therefore only two parameters are needed to describe the space wave efficiency: ε_r and h/λ_0. A first estimate of η uses a linear h/λ_0 dependence:

$$\eta = 1\cdot0 - \sqrt{(\varepsilon_r - 1)}\left(\frac{h}{\lambda_0}\right) \times 3\cdot4 \qquad (2)$$

The factor $\sqrt{(\varepsilon_r - 1)}$ in the second term assures that $\eta = 1$ for an air dielectric, and that η decreases faster with increasing h/λ_0 as ε_r increases. Eqn. 2 can also be written in terms of the cutoff frequency of the first-order TE mode:

$$\eta = 1\cdot0 - \left(\frac{f}{f_{c1}}\right)\left(\frac{3\cdot4}{4}\right) \qquad (3)$$

with $f_{c1} = c_0/[4h\sqrt{(\varepsilon_r - 1)}]$.
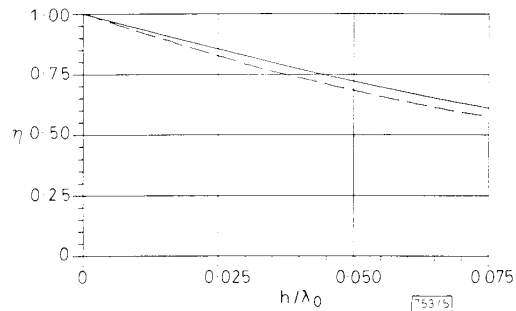
Fig. 5 *Space wave efficiency for wide patch antenna on substrate with* $\varepsilon_r = 4\cdot0$
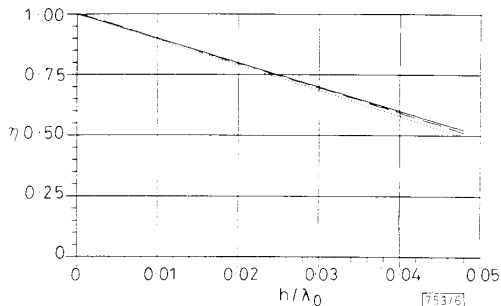
– – – – patch[5] ——— eqn. 4

From Figs. 2 and 3, we see that the linear dependence works well for small h/λ_0 (until 0·06), but that for larger substrate thicknesses and small ε_r some extra terms are needed. (For $\varepsilon_r = 12\cdot8$ the linear curve is extended practically to the point where the TE$_1$ mode can propagate.) The final expression for η is

$$\eta = 1\cdot0 - 3\cdot4H + \frac{1600}{\varepsilon_r^3}(H^3 - 100H^{5\cdot6}) \qquad (4)$$

with $H = \sqrt{(\varepsilon_r - 1)}(h/\lambda_0) = 0\cdot25(f/f_{c1})$.

In Figs. 2–6, the solid curve represents the results obtained with eqn. 4. As one can see, there is excellent agreement with the data from the Green function methods.

Range of validity: For practical purposes, it is largely sufficient if η can be calculated for $f < 0\cdot8f_{c1}$, which is equivalent to $H < 0\cdot20$. For $\varepsilon_r = 2\cdot55$ this corresponds to $h/\lambda_0 = 0\cdot16$, and for $\varepsilon_r = 12\cdot8$ to $h/\lambda_0 = 0\cdot058$. For this range of H a maximal

Fig. 6 *Space wave efficiency for wide and narrow patch antenna on substrate with* $\varepsilon_r = 9\cdot8$

– – – – patch[5] ········ dipole[5] ——— eqn. 4

difference of 0·04 is found between eqn. 4 and Pozar's results[1] for a patch 0·3 λ_0 wide (Figs. 2 and 3). A similarly small deviation of 0·05 is found between eqn. 4 and Perlmutter's[5] results (Figs. 4, 5 and 6). As the difference between η for dipoles and patches is always less than 0·02, eqn. 4 also holds for dipoles.

Conclusion: A very simple expression is presented that summarises the available data for space wave efficiency of rectangular microstrip antennas. Its arguments are ε_r and h/λ_0. The expression is valid for dipoles and patches, and has been checked against numerical data for $\varepsilon_r = 2\cdot2$, 2·55, 4, 9·8 and 12·8. The maximal difference between numerical data and the closed-form expression is 0·05 for $\sqrt{(\varepsilon_r - 1)}(h/\lambda_0) < 0\cdot20$.

B. NAUWELAERS   29th March 1989
A. VAN DE CAPELLE

Div. ESAT—TELEMIC
Katholieke Universiteit Leuven
Kardinaal Mercierlaan 94, B-3030 Leuven, Belgium

References

1 POZAR, D. M.: 'Considerations for millimeter wave printed antennas', *IEEE Trans.*, 1983, **AP-31**, pp. 740–747
2 ROUDOT, B., MOSIG, J. R., and GARDIOL, F. E.: 'Puissance et rendement associés aux antennes microruban'. Proc. JINA '89, Nice, France, 1989, pp. 232–236
3 BHATTACHARYYA, A. K., and GARG, R. G.: 'Effect of substrate on the efficiency of an arbitrarily shaped microstrip patch antenna'. *IEEE Trans.*, 1986, **AP-34**, pp. 1181–1188
4 PERLMUTTER, P., SHTRIKMAN, S., and TREVES, D.: 'Electric surface current model for the analysis of a microstrip rectangular element'. 1984 IEEE int. symp. digest on antennas and propagation, Boston, 1984, pp. 577–580
5 PERLMUTTER, P., SHTRIKMAN, S., and TREVES, D.: 'Electric surface current model for the analysis of microstrip antennas with application to rectangular elements', *IEEE Trans.*, 1985, **AP-33**, pp. 301–311
6 ROUDOT, B., TERRET, C., DANIEL, J. P., PRIBETICH, P., and KENNIS, P.: 'Fundamental surface-wave effects on microstrip antenna radiation'. *Electron. Lett.*, 1985, **21**, pp. 1112–1114
7 MOINI, R., HERAULT, J., and JECKO, B.: 'Influence des ondes de surface sur la puissance rayonnée par des antennes microruban'. Proc. JINA '89, Nice, France, 1989, pp. 260–263

PERFORMANCE ANALYSIS OF HIGH-DENSITY WDM SYSTEMS USING RAMAN AMPLIFICATION

Indexing terms: Optical communications, Optical fibres, Nonlinear optics, Multiplexing

The applications of Raman amplifiers as repeater amplifiers or post-transmitter amplifiers in a high-density WDM system are theoretically investigated. There exists an optimum pump power which results in maximum amplifier gain. The result shows that amplifier gains up to 50 dB and 20 dB are achievable for use as a repeater and a post-transmitter amplifier, respectively.

Introduction: High-density, wavelength-division-multiplexed (HDWDM) systems provide a means for exploiting the vast bandwidth of a single-mode fibre.[1] One of the limitations imposed on an HDWDM system is the power depletion caused by stimulated Raman scattering (SRS),[2,3] so that both the number of channels and transmission power are limited. On the other hand, SRS can be used to optically amplify multichannel signals with single pump power,[4] which is of special interest in an HDWDM system. The fibre Raman amplifier can be either used as a repeater amplifier to boost weak signals, or used at the transmitting end to amplify the multichannel signals so as to increase system transmission distance and relax the limitation caused by SRS. This letter investigates the application of Raman amplification in an HDWDM system.

Analysis: The nonlinear pumping process in an HDWDM system is complicated and depends on channel spacing, number of channels, as well as the pump and signal powers. Here we analyse the signals of an N-channel HDWDM fibre transmission system with Raman amplification, and consider the case that all signals are pulse-modulated while the pump is a continuous wave.

Let A and α denote the effective cross-section and loss coefficient of the fibre, respectively. To simplify the analysis, we assume that the Raman gain has a Lorentzian lineshape, while the actual lineshape in fibres is much more complicated.[5] The lineshape is given as

$$g(v_R) = \frac{g_0(w/2)^2}{(v_R - v_0)^2 + (w/2)^2} \quad (1)$$

where g_0 is the peak Raman gain coefficient, w the full width at half-maximum of the Lorentzian lineshape, v_R the Raman shift between the two coupling waves, and v_0 the Raman shift corresponding to the peak gain.

Let v_p and v_{si} denote the lightwave frequencies of the pump and the ith signal in the HDWDM system. In an HDWDM system the linewidths of the signals are much smaller than w, and hence the Raman gain for the signals is assumed to be constant. The Raman gain constant coupling the pump and the ith signal, g_i, and the gain constant coupling the ith and jth channels, g_{ij}, can then be calculated from eqn. 1 with appropriate v_R.

Let L denote the transmission distance. The signal power $S_i(0)$, $i = 1, 2, \ldots, N$, and the pump power $P(0)$ are injected at $z = 0$ and travel in the $+z$ direction. The differential equations governing the signals and the pump propagation are given by

$$\frac{dS_i(z)}{dz} = \left[-\alpha_s + \frac{g_i}{A} P_1(z) + \sum_{j=1}^{i-1} \frac{g_{ij} S_j(z)}{A} \right.$$
$$\left. - \sum_{m=i+1}^{N} \frac{v_{si}}{v_{sm}} \frac{g_{im} S_m(z)}{A} \right] S_i(z) \qquad i = 1, 2, \ldots, N \quad (2)$$

$$\frac{dP(z)}{dz} = -\left[\alpha_p + \sum_{i=1}^{N} \frac{g_i v_p}{A v_{si}} S_i(z) \right] P(z) \quad (3)$$

Here we assume $v_{s1} > v_{s2} \ldots > v_{sN}$ and that the N channels are equally spaced with channel spacing Δv. The second term in eqn. 2 denotes the coupling between the ith signal and the pump; the third and the last terms express the crosscoupling among the signal channels. Because of the crosscoupling among the signal channels, the optical power of the shorter-wavelength channels will be depleted by the longer-wavelength channels, and will be most severe for the shortest-wavelength channel (channel 1). As a result, the system transmission distance will be limited by the achievable amplifier gain of channel 1. Numerical calculation is carried out to estimate the achievable amplifier gain. We consider the worst case that all the channels are in the 'on' state, in which channel 1 is most depleted. For simplicity we choose an odd number of channels, and locate the middle channel at the centre of the Raman gain profile. The amplifier gain of channel 1 at $z = L$ is defined as

$$G = 10 \log \frac{S_1(L)}{S_1(0)e^{-\alpha L}} \quad (4)$$

where $S_1(L)$ is the power of channel 1 at $z = L$ with Raman amplification.

The relationship between the gain of channel 1 and the pump power is shown in Fig. 1. Here two regions can be characterised. One is the linear region in which G increases linearly with $P(0)$, while the other is the saturation region where G gradually reaches a maximum value and decreases as $P(0)$ further increases. For use as post-transmitter amplifiers ($S_i(0) = 0.1$ mW), the achievable gain is much smaller and the maximum gain occurs at a lower pump power level than those used as repeater amplifiers ($S_i(0) = 0.1$ μW). The influence of channel number N on G is shown in Fig. 2, where g_1 and the

total signal span $(N - 1)\Delta v$ are kept constant. The degradation of G as N increases is expected since more power of channel 1 is depleted. When used as repeater amplifiers, G is insensitive to the channel number N in the linear region but degrades in the saturation region. In the linear region, because channel 1 obtains much more power from the pump than that depleted by the other channels, G is nearly independent of N.
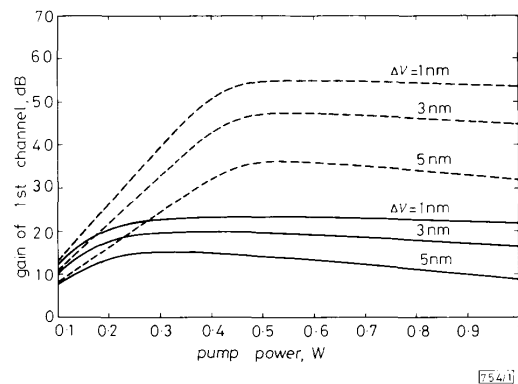
Fig. 1 *G as function of pump power for $N = 11$*

Solid lines (post-transmitter amplifiers): $S_i(0) = 0.1$ mW; broken lines (repeaters): $S_i(0) = 0.1$ μW. For convenience we use wavelength unit for Δv. $g_0 = 7.5 \times 10^{-14}$ m/W, $A = 5 \times 10^{-11}$ m², $\alpha = 0.2$ dB/km, $W = 240$ cm⁻¹, $v_0 = 460$ cm⁻¹, $L = 150$ km

However, in the saturation region the depletion by the other channels becomes comparable to that obtained from the pump, and thus degradation results. Since it is essentially operating in the saturation region when used as a post-transmitter amplifier, G degrades as N increases. When the pump power increases, the signal power of channel 1 depleted by the other channels may exceed that obtained from the pump, so that the gain decreases. Therefore there exists an optimum pump power which results in maximum gain of channel 1. As shown in the Figures, for use as a repeater amplifier, an amplifier gain up to 50 dB is achievable, which corresponds to 250 km repeater spacing for 0.2 dB/km fibre loss. For use as a post-transmitter amplifier, more than 20 dB gain is still obtainable, corresponding to 100 km extended transmission length, and the constraint imposed by Raman crosstalk is relaxed because the depleted power of channel 1 by the other channels is compensated by the pump.
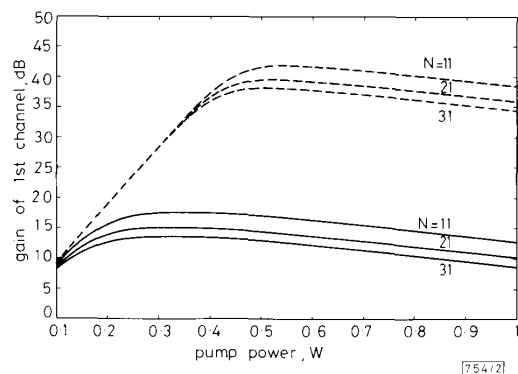
Fig. 2 *Effect of channel number on G*

Solid lines (post-transmitter amplifiers): $S_i(0) = 0.1$ mW; broken lines (repeaters): $S_i(0) = 0.1$ μW. Same parameters used as in Fig. 1; $(N - 1)\Delta v = 40$ nm

Conclusions: We have investigated the properties of Raman amplification in an HDWDM system. The results show that there exists an optimum pump power to yield a maximum amplifier gain. A high gain is achievable for use as a repeater amplifier, and a modest gain is obtainable when used as a post-transmitter amplifier. Based on these results, we conclude

698

that Raman amplifiers are potential candidates to amplify multichannel signals in an HDWDM system.

M.-S. KAO   *29th March 1989*
J. WU

Department of Electrical Engineering
National Taiwan University
Taipei, Taiwan 10764, Republic of China

References

1 KOBRINSKI, H., *et al.*: 'Demonstration of high capacity in the LAMBDANET architecture: a multiwavelength optical network', *Electron. Lett.*, 1987, **23**, pp. 824–826
2 CHRAPLYVY, A. R., and HENRY, P. S.: 'Performance degradation due to stimulated Raman scattering in wavelength-division-multiplexed optical fibre systems', *ibid.*, 1983, **19**, pp. 641–643
3 CHRAPLYVY, A. R.: 'Limitations on lightwave communications imposed by optical fiber nonlinearities'. Tech. dig. opt. fiber commun. conf., 1988, p. 19
4 EDAGAWA, N., *et al.*: 'Simultaneous amplification of wavelength-division-multiplexed signals by a highly efficient fibre Raman amplifier pumped by high-power semiconductor lasers', *Electron. Lett.*, 1987, **23**, pp. 196–197
5 STOLEN, R. H., and IPPEN, E. P.: 'Raman gain in glass optical waveguides', *Appl. Phys. Lett.*, 1973, **22**, pp. 276–278

FEMTOJOULE BISTABLE OPTICAL SWITCHING OF INHOMOGENEOUSLY PUMPED LASER DIODE AT 500 MHz USING MODE-LOCKED TUNABLE DIODE LASER

Indexing terms: Semiconductor lasers, Optical switching, Nonlinear optics

We have investigated the nonlinear transfer characteristics and temporal response of bistable three-section lasers within a broad wavelength interval (30 nm), when switched with picosecond optical pulses (20 ps) at a high repetition rate. The minimum input coupled switch-on energy was 0·7 fJ. The shortest switching time was 60 ps.

In this letter we present results comparable to the lowest switching energies,[1] and at the same time the highest repetition rates[2] reported for bistable optical devices.

Experiment: The bistable laser diode (BLD) was a three-section GaInAsP diode, with a lasing wavelength of 1310 nm. The absorber section was situated at the facet where the optical switching pulses were incident. The bias currents were chosen so that the BLD was kept 0·1 mA below the electrical switch-on threshold. Further details can be found in Reference 3.

We measured the photocurrent generated in the BLD when it was reverse biased to optimise and evaluate the input coupling efficiency, which was approximately 10%. A pinhole transmission measurement of the input spot size was in very good agreement with this input coupling efficiency.

A mode-locked diode laser was employed for switching the BLD. The mode-locked laser produced optical pulses of 20–40 ps FWHM, as measured by autocorrelation. These pulses were monitored on a sampling oscilloscope by using a *pin* photodiode with a rise time of 60 ps. The wavelength of the mode-locked laser was controlled by a Fabry–Perot étalon placed in an external cavity. The spectral width of the pulses was ≤3 Å for wavelengths less than 1300 nm and ≤5 Å for longer wavelengths.

To achieve fast switch-off 1 ns after the set-pulse, a short negative electrical pulse was employed to extract the charge carriers from the absorber section.[2] The pulse amplitude was around 20 mA and the pulse width was less than 130 ps (FWHM).

Minimum switching energy: We measured the minimum input energy for switching E_{min} in front of the microscope objective

for input coupling (NA = 0·83). The output energy E_{output}, when switching with minimum input energy, was measured after the microscope objective for output coupling (NA = 0·25). The results are plotted against input wavelength in Fig. 1. We found the smallest E_{min} to be 7·2 fJ, i.e. the input coupled energy was approximately 0·7 fJ, at an input wavelength of 1305·8 nm. This corresponds to less than 5000 input coupled photons. Another feature of the switching characteristics at 1305·8 nm is the high output energy 170 fJ. This optimum wavelength was 4 nm shorter than the main lasing mode of the BLD. We recorded the input and output spectra using a monochromator with a resolution better than 1 Å. There were three common features of all the output spectra obtained: (*a*) the attenuated transmitted input signal, (*b*) an initial lasing BLD-mode positioned quite near the input wavelength of (*a*), and (*c*) a broad dominating laser spectrum of the BLD which was centred at 1310 nm. This implies that the BLD reaches the steady-state within 1 ns.
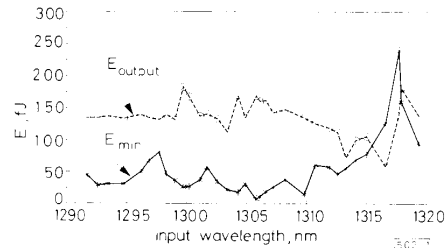

Fig. 1 *Minimum switching energy E_{min} plotted against input wavelength*

Output energy E_{output} corresponds to input energy E_{min}

We investigated resonance effects by increasing the number of sampled input wavelengths within the interval for optimum switching energy. This was accomplished by temperature-tuning the mode-locked laser. The BLD was switched at several input wavelengths in the interval 1304·8–1306·1 nm and with a spectral width of the mode-locked laser pulse of around 1·5 Å (FWHM). This was plotted with E_{min} and E_{output} against input wavelength, as in Fig. 1. The investigated interval was larger than the spacing of two internal cavity modes of the BLD. The wavelength difference of the reflected input pulse and the output pulse was simultaneously measured via a beam splitter placed between the mode-locked laser and the BLD. We found no clear resonant behaviour in this interval.

Transfer function: In Fig. 2, we have plotted E_{output} against E_{input} for three different input wavelength intervals. The five points in the Figures are the mean values, within each of the three intervals, obtained for E_{input} equal to 0, $E_{min}/2$, E_{min}, $2E_{min}$ and $4E_{min}$, respectively. To obtain a measure of the spread of results within different input wavelength intervals, we calculated the standard deviations, which were plotted as error bars for E_{output} and E_{min} and E_{min} at each point. The nonlinear shape of the transfer characteristics is more pronounced for the optimum wavelength interval than for long wavelengths, as in Figs. 2*b* and *c*. The threshold behaviour observed in all three intervals confirms that we have true bistable switching at 500 MHz. Although the set-up was not optimised for output coupling, the maximum pulse energy gain was 14 dB.

Bistable switching time: The shortest deconvolved rise time of the BLD signal was approximately 60 ps when switching in the optimum wavelength interval with a high input energy. The BLD signal rises immediately after the input signal. The input coupled energy could be decreased to 29 fJ without increasing the switching time. The maximum delay time was 0·7 ns, limited by the electrical reset 1 ns after the input pulse.

Summary: We have characterised bistable switching of a three-section bistable laser diode in an input wavelength interval of 30 nm and at a repetition rate of 500 MHz. Bistable switching was performed with less than 5000 input coupled photons. The shortest recorded bistable switching time was approximately 60 ps.